



## OPEN The Atlantic Cod MHC I compartment has the properties needed for cross-presentation in the absence of MHC II

Synne Arstad Bjørnstad<sup>1</sup>, Monica Hongrø Solbakken<sup>1,2</sup>, Pia Krokene<sup>1</sup>, Bernd Thiede<sup>1</sup>, Ketil Hylland<sup>1</sup>, Kjetill S. Jakobsen<sup>1</sup>, Sissel Jentoft<sup>1</sup>, Oddmund Bakke<sup>1</sup> & Cinzia Progida<sup>1</sup>✉

Atlantic cod has a peculiar immune system, characterized by the loss of Major Histocompatibility Complex (MHC) class II pathway, and an extreme expansion of the MHC class I gene repertoire. This has led to the hypothesis that some of the MHC I variants have replaced MHC II by presenting exogenous-peptides in a process similar to cross-presentation. In mammals, MHC I loads endogenous antigens in the endoplasmic reticulum, but we recently found that different Atlantic cod MHC I gene variants traffic to endolysosomes. There, they colocalize with Tapasin and other components of the peptide-loading complex, indicating a plausible peptide-loading system outside the endoplasmic reticulum. In this study, we further characterize the identity of the Atlantic cod MHC I compartment (cMIC). We found that, similarly to mammalian MHC II compartment, cMIC contains late endosomal markers such as Rab7, LAMP1 and CD63. Furthermore, we identified Hsp90b1 (also known as grp94) and LRP1 (also known as CD91) as interactors of MHC I by mass spectrometry. As these two proteins are involved in cross-presentation in mammals, this further suggests that Atlantic cod MHC I might use a similar mechanism to present exogenous peptides, thus, compensating for the absence of MHC II.

Major histocompatibility complex (MHC) class I and II play a critical role in the adaptive immune system of jawed vertebrates including teleosts<sup>1,2</sup>. MHC I and II share the function of presenting small peptide fragments at the cell surface to CD8<sup>+</sup> or CD4<sup>+</sup> T-cells, respectively<sup>3</sup>. While both complexes present peptide fragments, the intracellular traffic of the complexes and thus the origin of the peptide fragments they bind to are different. MHC I binds in the endoplasmic reticulum (ER) peptide fragments that originate from inside the cell, called endogenous peptides. The complex is then transported to the plasma membrane through the secretory pathway<sup>3</sup>. MHC II on the other hand binds peptide fragments originating from the outside of the cell, called exogenous peptides. This occurs in specialized late endosomal compartments named MHC II compartment (MIIC)<sup>3</sup>. MHC II is unable to bind peptides in the ER because it associates with the chaperon invariant chain (Ii), which targets MHC II to late endosomes. Here, Ii is degraded and MHC II can bind exogenous peptides. Once MHC II-peptide complexes are formed, they are transported to the plasma membrane<sup>3</sup>. A link between the two pathways exists as MHC I can traffic to endosomal compartments where it binds exogenous peptides. This process is known as cross-presentation and involves either the cytosolic or vacuolar pathway<sup>4</sup>. While the cytosolic pathway depends on translocation of antigens from the endosomal lumen to the cytosol for proteasomal degradation and then back to the endosomal lumen for MHC I loading, the vacuolar pathway depends on antigen degradation within the endosomal lumen by endosomal proteases<sup>4</sup>. Interestingly, while exogenous antigen loading of MHC II is facilitated by low acidity and high proteolytic activity of MIICs, MHC I cross-presentation is primarily associated with loading in endosomes with neutral luminal pH and reduced proteolytic activity<sup>5,6</sup>. Indeed, cross-presentation in mammals is primarily performed by dendritic cells due to adaptation of their endosomal system with reduced endosomal acidification and decreased proteolytic capacity<sup>7</sup>.

MHC I and II emerged in jawed vertebrates around 500 million years ago<sup>8</sup>. Until recently, it was believed that the MHC I and II pathways were conserved features of the vertebrate immune system, due to their importance in proper T-cell response. However, several reports have demonstrated that there exist some teleost species or even lineages where entire (or parts of the) MHC II pathway is functionally lost<sup>9–14</sup>. One striking example is the Atlantic cod (*Gadus morhua*) that lacks MHC II genes, including the MHC II-interacting molecule CD4, necessary for T cell activation, and Ii<sup>9</sup>. These findings have later been confirmed with improved Atlantic cod

<sup>1</sup>Department of Biosciences, University of Oslo, Oslo, Norway. <sup>2</sup>Present address: Norwegian University of Life Sciences, Ås, Norway. ✉email: c.a.m.progida@ibv.uio.no

genome assemblies<sup>15</sup>, genome sequencing of Atlantic haddock<sup>16</sup>, as well as large scale teleost genome assemblies demonstrating that the loss of the MHC II pathway occurred around 80–100 Mya at the very base of the Gadiformes radiation<sup>14</sup>.

While Atlantic cod lack the MHC II pathway, it is characterized by an expanded MHC I gene repertoire with 80–100 predicted gene copies<sup>9,14</sup>. Little is known on the function of this genetic expansion. One hypothesis is that parts of the expanded MHC I repertoire function more like MHC class II by entering late endosomal compartments for binding exogenous peptides. In line with this hypothesis, we have recently demonstrated that five Atlantic cod MHC class I gene variants, representing the most common MHC I cytosolic tail configurations in the MHC I gene repertoire, localize to endolysosomes in the Atlantic cod larval (ACL) cell line<sup>17</sup>. This is intriguing as in mammals MHC class I mainly localizes to the plasma membrane, while MHC class II localizes to specialized endolysosomes or MIIC<sup>3</sup>. The localization of Atlantic cod MHC I to endolysosomes suggests that it can perform cross-presentation, which is further supported by the presence of peptide loading complex (PLC) components such as Tapasin, and the Transporter associated with antigen processing 1 and 2 (TAP1/2) on the MHC I positive compartment<sup>17</sup>.

The MIIC in mammals is a specialized organelle of the endocytic pathway found in antigen presenting cells where MHC class II binds exogenous antigens<sup>3,18</sup>. It is characterized by acidic pH, the presence of proteases like cathepsins S and L, and it is positive for the late endosomal markers LAMP1 and CD63<sup>19–23</sup>. Based on our previous findings<sup>17</sup>, we hypothesized that Atlantic cod MHC I compartment (cMIC) is similar to the MIIC in mammals. Here, we further characterized the identity of cMIC in Atlantic cod larval (ACL) cell line and validate our findings in primary hepatocytes and leukocytes isolated from wild-caught Atlantic cod. We found that, similarly to mammalian MIIC, cMIC is an organelle positive for late endosomal markers such as Rab7, LAMP1 and CD63<sup>19,20,24</sup>. Furthermore, we identified Hsp90b1 (also known as grp94) and LRP1 (also known as CD91) as interactors of MHC I by mass spectrometry analysis. As these two proteins are involved in cross-presentation in mammals<sup>25,26</sup>, our findings further suggest that Atlantic cod MHC I might use a similar mechanism to present exogenous peptides thus compensating for the absence of MHC II.

## Results

### The Atlantic Cod MHC I compartment is a late endosomal compartment

We have previously demonstrated that five Atlantic cod MHC I variants, differently from mammalian MHC I, all localize to acidic compartments<sup>17</sup>. To further characterize the identity of the Atlantic cod MHC I-positive compartment (cMIC), we selected one of these MHC I variants and expressed it together with a panel of early-, recycling-, late endosomal and lysosomal markers in the epithelial-like Atlantic cod larval (ACL) cell line<sup>27</sup>. From super-resolution microscopy analysis, MHC I-GFP showed higher degree of co-localization with late endosomal and lysosomal markers such as BFP-Rab7A, RFP-Rab9, mCherry-LIMP2, LAMP1-GFP and CD63-GFP (Manders' coefficients  $\geq 0.75$ , Fig. 1A, C; Suppl. Figure 1A–D), than with the early endosomal marker mCherry-Rab5 (Manders' coefficient 0.4, Fig. 1A, C), or the recycling marker mApple-Rab11 (Manders' coefficient 0.2, Fig. 1B, C). Co-localization analysis with additional early or recycling molecular markers such as GFP-Rab14, GFP-Rab22, HRS-YFP and RFP-SNX1, further confirmed a low degree of colocalization between MHC I-GFP and these compartments (Manders' coefficients  $< 0.25$ , Fig. 1C; Suppl. Figure 2 A–D).

To strengthen our finding that Atlantic cod MHC I indeed localizes to late endosomes, we verified this in primary cells derived from wild-caught Atlantic cod. We used primary hepatocytes, as these cells have been successfully transfected in other marine fish species<sup>28</sup>, and leukocytes from Atlantic cod, to investigate if MHC I localization could be different in immune-derived cells. RNA profiles from different Atlantic cod tissues confirm ubiquitous MHC I expression (Suppl. Figure 3) similar to mammalian MHC I<sup>29</sup>. Primary cells were transfected with MHC IGFP and labelled with lysotracker red, a fluorescent dye that accumulates in acidic compartments. The results show that MHC I-GFP colocalizes with lysotracker red in both hepatocytes and leukocytes (Fig. 2A,B,E–G) which is in line with the findings in ACL cells<sup>17</sup>.

We then co-transfected primary cells with MHC IGFP and mApple-Rab7A and analysed the colocalization between the two proteins. The results show that MHC I is present on Rab7A-positive endosomes in primary hepatocytes (Fig. 2C–E) and leukocytes (Fig. 2H–I), thus validating the cMIC as a late endosomal/lysosomal compartment in primary cells derived from cod. Interestingly, small intraluminal MHC I vesicles were observed inside large mApple-Rab7A positive endosomes in primary leukocytes (Fig. 2H, J–K), indicating that MHC I localizes to multivesicular bodies (MVBs), similarly to MHC II in mammals<sup>30,31</sup>.

### *Francisella noatunensis* ssp. *noatunensis* escapes cMIC

To understand if internalized pathogens enter the cMIC, and if Atlantic cod MHC I relocates upon infection as known for mammalian MHC I in cross-presentation<sup>32</sup>, we infected ACL cells with *Francisella noatunensis* subsp. *noatunensis* (*Fnn*), the causative agent of francisellosis in Atlantic cod<sup>33</sup>. *Fnn* is a facultative intracellular bacterium, which similarly to the human pathogen *Francisella tularensis*<sup>34</sup>, seems to be able to escape the endosomal pathway to avoid lysosomal degradation<sup>35</sup>. ACL cells co-transfected with MHC I-GFP and BFP-Rab7A were infected with *Fnn* expressing mCherry for 6 h and analysed by super-resolution microscopy. The results show that internalized *Fnn* mCherry is present in MHC I-GFP and BFP-Rab7A-positive cMICs (Fig. 3A,B). Colocalization analysis between MHC I-GFP and BFP-Rab7A in *Fnn* infected cells indicates a small but not significant reduction compared to non-infected cells (Fig. 3C) suggesting that Atlantic cod MHC I does not relocate upon bacterial infection. However, 3D super-resolution microscopy shows that *Fnn* escapes MHC I-GFP and BFP-Rab7A-positive compartments, revealing that cMIC is an endosomal compartment that *Fnn* is able to escape (Fig. 3A).

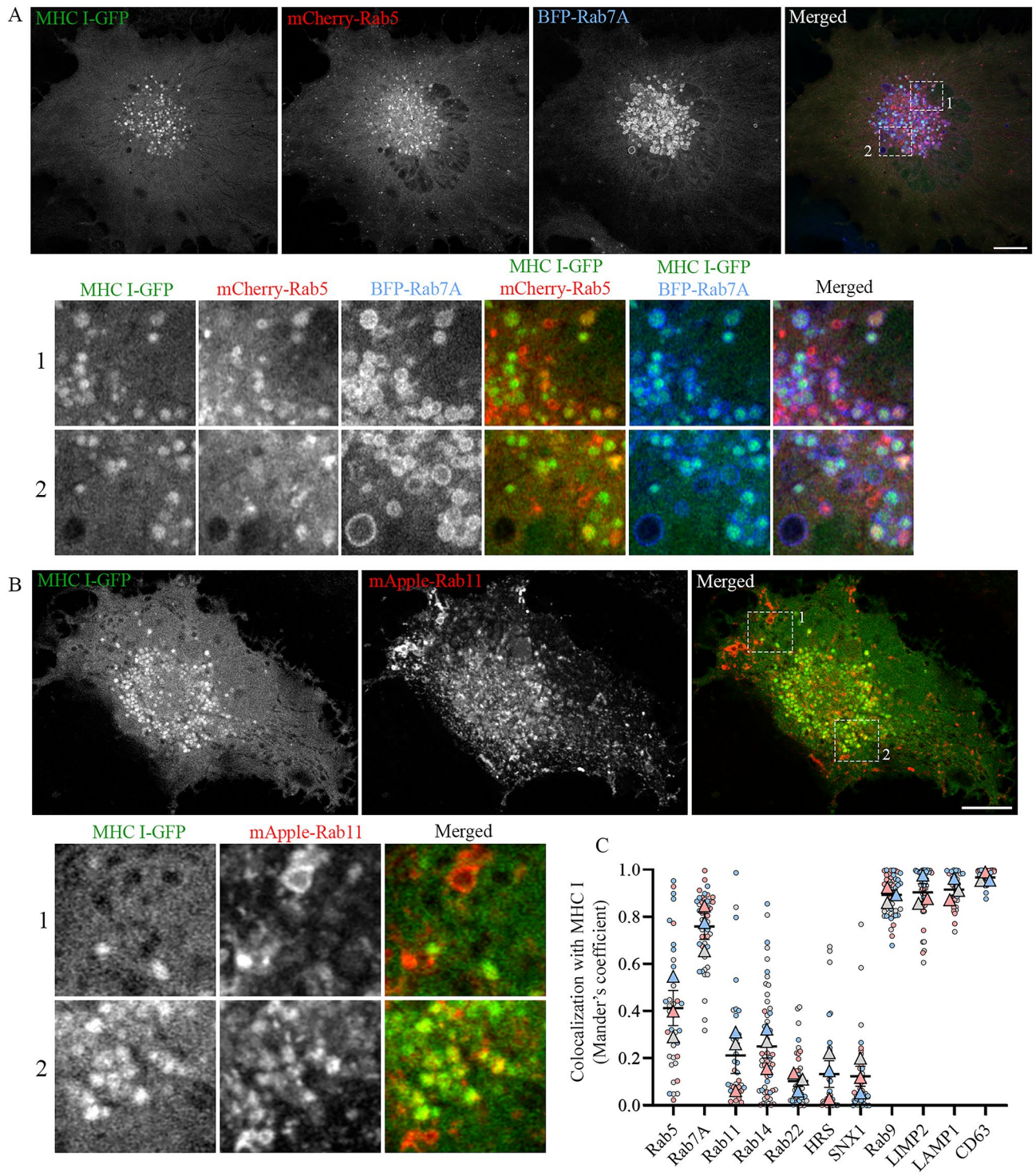
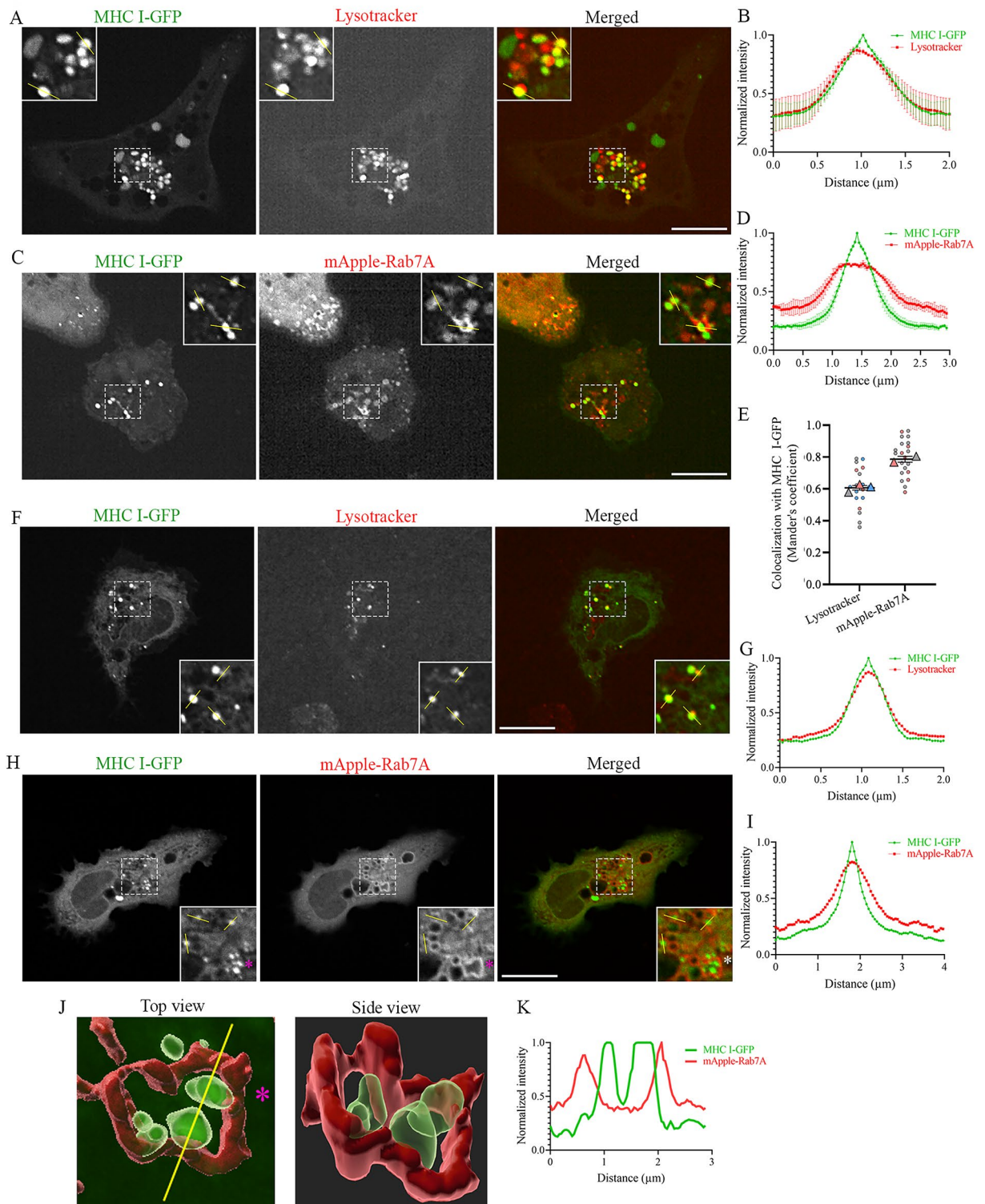


**Fig. 1.** Atlantic cod MHC I colocalizes more with late endosomal and lysosomal markers than early and recycling endosomal markers in ACL cells. (A) Representative image of an ACL cell transiently co-transfected with MHC I-GFP, mCherry-Rab5 and BFP-Rab7A. Cells were imaged using a Zeiss LSM880 Fast AiryScan microscope. Scale bar: 10  $\mu$ m. Magnifications of boxed areas 1 and 2 are shown below. (B) Representative image of an ACL cell transiently co-transfected with MHC I-GFP and mApple-Rab11. Cells were imaged using a Zeiss LSM880 Fast AiryScan microscope. Scale bar: 10  $\mu$ m. Magnifications of boxed areas 1 and 2 are shown below. (C) The graph represents colocalization analysis between Atlantic cod MHC I-GFP and the indicated endosomal and lysosomal markers. Colocalization was analysed by calculating Manders' coefficient in ImageJ. Scatter plot shows the mean  $\pm$  SEM from three independent experiments, colour coded for each experimental repeat. Dots represent individual measurements and are colour coded according to experimental repeat.  $n > 32$  cells.



### Atlantic Cod MHC I does not traffic to cMICs via the plasma membrane

After determining that the cMIC is a late endosomal compartment, we wanted to investigate how MHC I reaches this compartment. While human MHC I is predominantly found at the plasma membrane, its location is not static<sup>17,36</sup>. MHC I is constantly internalized by different endocytic pathways, including both clathrin-dependent and -independent pathways, for destruction or recycling<sup>37,38</sup>. In mammals, the origin of MHC I in cross-presentation is a matter of debate<sup>39</sup>, but MHC I can enter the endolysosomes either by uptake from the cell surface through endocytosis<sup>40</sup>, or be actively transported by binding Ii in the ER<sup>36,41</sup>.

To understand if Atlantic cod MHC I is transported to cMICs via the plasma membrane, we inhibited endocytosis by using Dynasore, a drug that prevents the activity of Dynamin<sup>42,43</sup>. Dynamin is important for membrane tubulation and fission of budding vesicles, and is essential for clathrin-mediated endocytosis, but also for caveolae-mediated endocytosis, a type of clathrin-independent pathway<sup>44,45</sup>. First, we tested the drug in ACL

◀ **Fig. 2.** Atlantic cod MHC I localizes to late endosomes/lysosomes in primary hepatocytes and leukocytes. (A) Representative image of an Atlantic cod primary hepatocyte transiently transfected with Atlantic cod MHC I-GFP. Cells were stained using lysotracker red and imaged using an Olympus SpinSR SoRA microscope. Scale bar: 10  $\mu\text{m}$ . Magnification of boxed area is shown as inset. The yellow lines illustrate regions selected for fluorescence intensity profile analysis. (B) The graph shows the normalized fluorescence intensity profiles relative to MHC I-GFP and lysotracker represented as mean  $\pm$  SEM ( $n=90$  vesicles from 17 cells from three fish specimens). (C) Representative image of Atlantic cod primary hepatocyte transiently co-transfected with MHC I-GFP and mApple-Rab7A. Cells were imaged using an Olympus SpinSR SoRA microscope. Scale bar: 10  $\mu\text{m}$ . Magnification of boxed area is shown as inset. The yellow lines illustrate regions selected for fluorescence intensity profile analysis. (D) The graph shows the normalized fluorescence intensity profiles relative to MHC I-GFP and mApple-Rab7A represented as mean  $\pm$  SEM ( $n=158$  vesicles from 24 cells from two fish specimens). (E) The graph represents colocalization analysis between Atlantic cod MHC I-GFP and lysotracker or mApple-Rab7A. Colocalization was analysed by calculating Manders' coefficient in ImageJ. Scatter plot shows the mean  $\pm$  SEM from  $n \geq 18$  cells (from at least two fish, colour coded for each experimental repeat). Dots represent individual measurements and are colour coded according to experimental repeat. (F) Representative image of an Atlantic cod primary leukocyte transiently transfected with MHC I-GFP and stained using lysotracker red. Cells were imaged using an Olympus SpinSR SoRA microscope. Scale bar: 10  $\mu\text{m}$ . Magnification of boxed area is shown as inset. The yellow lines illustrate regions selected for fluorescence intensity profile analysis. (G) The graph shows the normalized fluorescence intensity profiles relative to MHC IGFP and lysotracker represented as mean ( $n=79$  vesicles from 8 cells from one fish). (H) Representative image of an Atlantic cod primary leukocyte transiently co-transfected with MHC IGFP and mApple-Rab7A. Cells were imaged using an Olympus SpinSR SoRA microscope. Scale bar: 10  $\mu\text{m}$ . Magnification of boxed area is shown as inset. The yellow lines illustrate regions selected for fluorescence intensity profile analysis. The purple asterisk indicates a large Rab7A positive vesicle, with three intraluminal MHC I-positive vesicles. (I) The graph shows the normalized fluorescence intensity profiles relative to MHC IGFP and mApple-Rab7A represented as mean ( $n=99$  vesicles from 20 cells from one fish). (J) Imaris isosurface 3D rendering of the large mApple-Rab7A-positive vesicle containing MHC I-GFP intracellular vesicles from the image in (H) (marked with the purple asterisk). The yellow line illustrates the region used to generate the fluorescence intensity plot shown at the right. (K) The graph shows the normalized fluorescence intensity profile relative to MHC IGFP and mApple-Rab7A from the vesicle in (J).

cells by analysing the uptake of epidermal-growth-factor (EGF)-Alexa555. In untreated cells, EGF-Alexa555 was successfully internalized in lysotracker-positive compartments, while the uptake of EGF-Alexa555 was prevented in ACL cells treated with Dynasore, resulting in accumulation of EGF-Alexa555 at the cell surface (Fig. 4A). Having validated that Dynasore prevents endocytosis in ACL cells, we then investigated whether it affects MHC I localization in ACL cells transfected with MHC I-GFP. The results show no accumulation of MHC IGFP at the plasma membrane in Dynasore-treated cells compared to untreated cells (Fig. 4B), indicating that Atlantic cod MHC I is not transported to late cMICs via dynamin-dependent endocytosis.

We also investigated if MHC I could be internalized by a dynamin-independent pathway such as by macropinocytosis<sup>46</sup> using 5-N-ethyl-N-isopropyl amiloride (EIPA), a drug that inhibits macropinocytosis<sup>47,48</sup>. We validated EIPA blockage in ACL cells by analysing uptake of 70 kDa dextran-TexasRed. In untreated cells, dextran was internalized in lysotracker-positive compartments, while its uptake was prevented in EIPA-treated cells, resulting in accumulation at the cell surface (Fig. 4C, D). As EIPA prevents macropinocytosis in ACL cells, we then examined its effects on MHC I localization in ACL cells transfected with MHC I-GFP. Even though we did observe a reduction in overlap between MHC I-GFP and lysotracker in EIPA treated cells (Fig. 4D), possibly as consequence of the known secondary effects of EIPA on endolysosomal pH and trafficking<sup>49,50</sup>, the results show no accumulation of MHC I-GFP at the plasma membrane in EIPA-treated cells compared to untreated cells (Fig. 4C).

Altogether, these results indicate that Atlantic cod MHC I does not traffic to cMICs via the plasma membrane by dynamin-dependent endocytosis nor by macropinocytosis.

### LRP1 is a novel Atlantic cod MHC I interactor that localizes to cMIC

To further characterize the composition of the cMIC, we immunoprecipitated MHC I from ACL cells transfected with MHC I-GFP using GFP-Trap beads. GFP transfected cells were used as control and the immunoprecipitated samples were analysed by mass spectrometry. Among the proteins that have high spectral counts with MHC I-GFP and none with GFP alone are Atlantic cod orthologs of known mammalian MHC I interactors, such as Transporter associated with antigen processing 1 (Tap1), TAP binding protein like (TAPBPL/Tapasin-related protein) and calnexin (CANX) (Fig. 5A, Suppl. Figure 5A). These are all components of the peptide loading complex (PLC) necessary for proper MHC I assembly and peptide-loading<sup>51</sup>. In addition to known MHC I interactors, several proteins whose mammalian orthologs are trafficking proteins (Rab6A, Rab5C, Rab18, Rab15, Rab13, KNT1, EHD4, DNMT2, CDC42) and adaptors (AP-1, AP-2, AP-3) were detected. Cathepsin F (CTSF), a late endosomal/lysosomal enzyme was also identified, which is interesting due to its role in proper peptide loading of MHC class II in humans<sup>52-54</sup>. Amongst other interesting and novel interactors, the LDL-receptor related protein 1 (LRP1, also known as CD91), Heat shock protein 90 b1 (Hps90b1 also known as grp94/gp96/endoplasmic) and CMTM6, were identified. While the first two are reported to have a function in cross presentation<sup>55-59</sup>, the latter is a transmembrane protein<sup>60</sup> that works in recycling of receptors to prevent their lysosomal degradation<sup>61,62</sup>. To validate the interactors identified by mass spectrometry, western blot analysis was

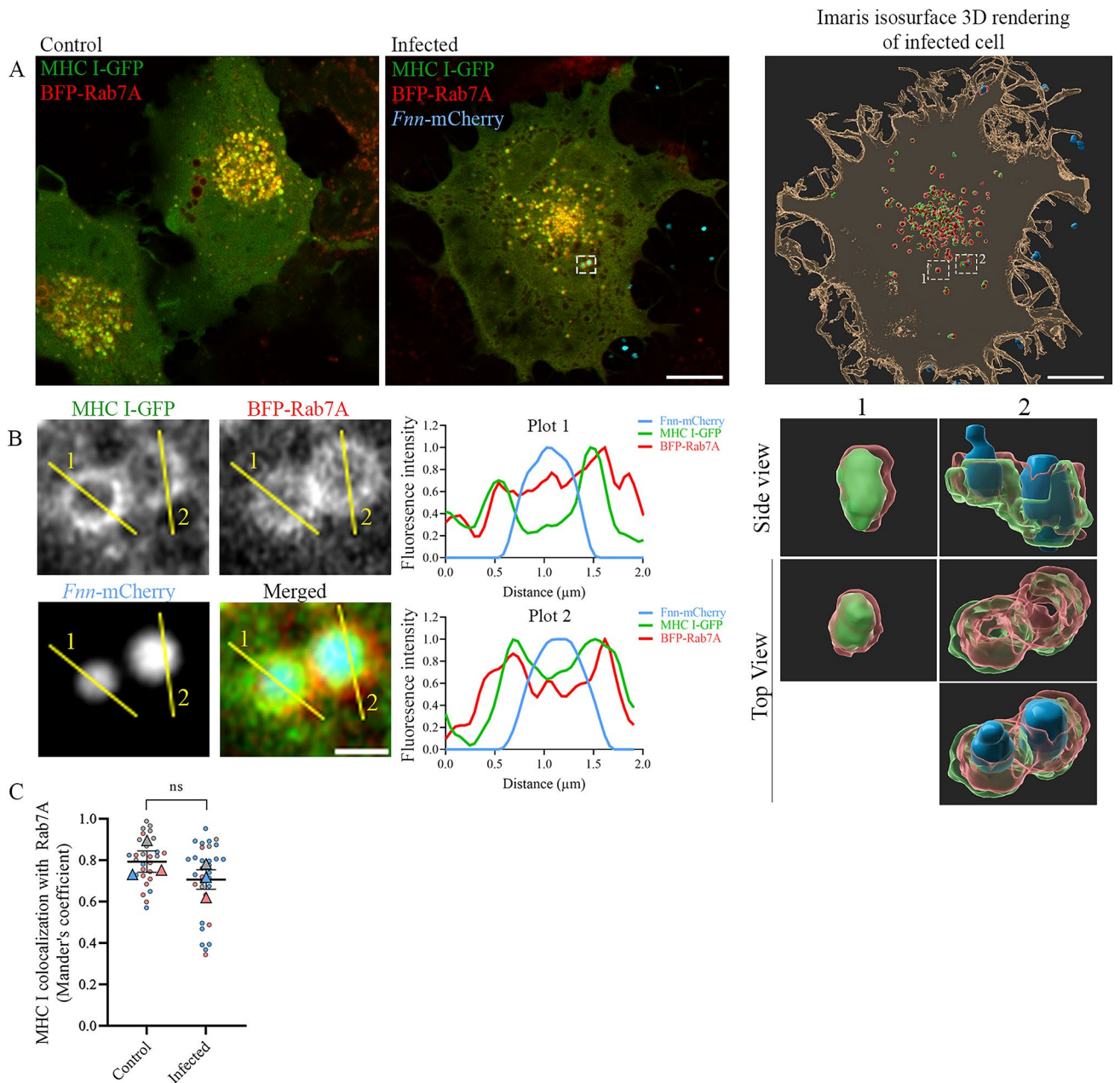


**Fig. 3.** *Francisella noatunensis* ssp. *noatunensis* localizes to and escapes cMIC. **(A)** Representative images of ACL cells transiently co-transfected with MHC I-GFP and BFP-Rab7A before and after infection with *Francisella noatunensis* ssp. *noatunensis* (*Fnn*) stable expressing mCherry. Cells were imaged using a Zeiss LSM880 Fast AiryScan microscope. Scale bar: 10  $\mu$ m. Imaris isosurface 3D rendering is shown for the infected cell (right) including magnifications of the insets. Inset 1 illustrates an intact and non-infected endosome. Inset 2 shows *Fnn*-containing endosomes that are opened (as visible from the top view), with the internalized bacteria (in blue) protruding from these endosomes (as visible from the side view), thus escaping from the infected endosomes. Scale bar: 10  $\mu$ m. **(B)** Magnification of the boxed area from **(A)**. Scale bar: 1  $\mu$ m. The graphs show the normalized fluorescence intensity profiles along the two yellow lines (plot 1 and 2) for *Fnn*-mCherry, MHC I-GFP and BFP-Rab7A. **(C)** The graph represents colocalization analysis between MHC I-GFP and BFP-Rab7A in control or *Fnn*-mCherry infected ACL cells. Colocalization was analysed by calculating Manders' coefficient in ImageJ. Scatter plot shows the mean  $\pm$  SEM from three independent experiments, colour coded for each experimental repeat ( $n \geq 29$  cells). Dots represent individual measurements and are colour coded according to experimental repeat.

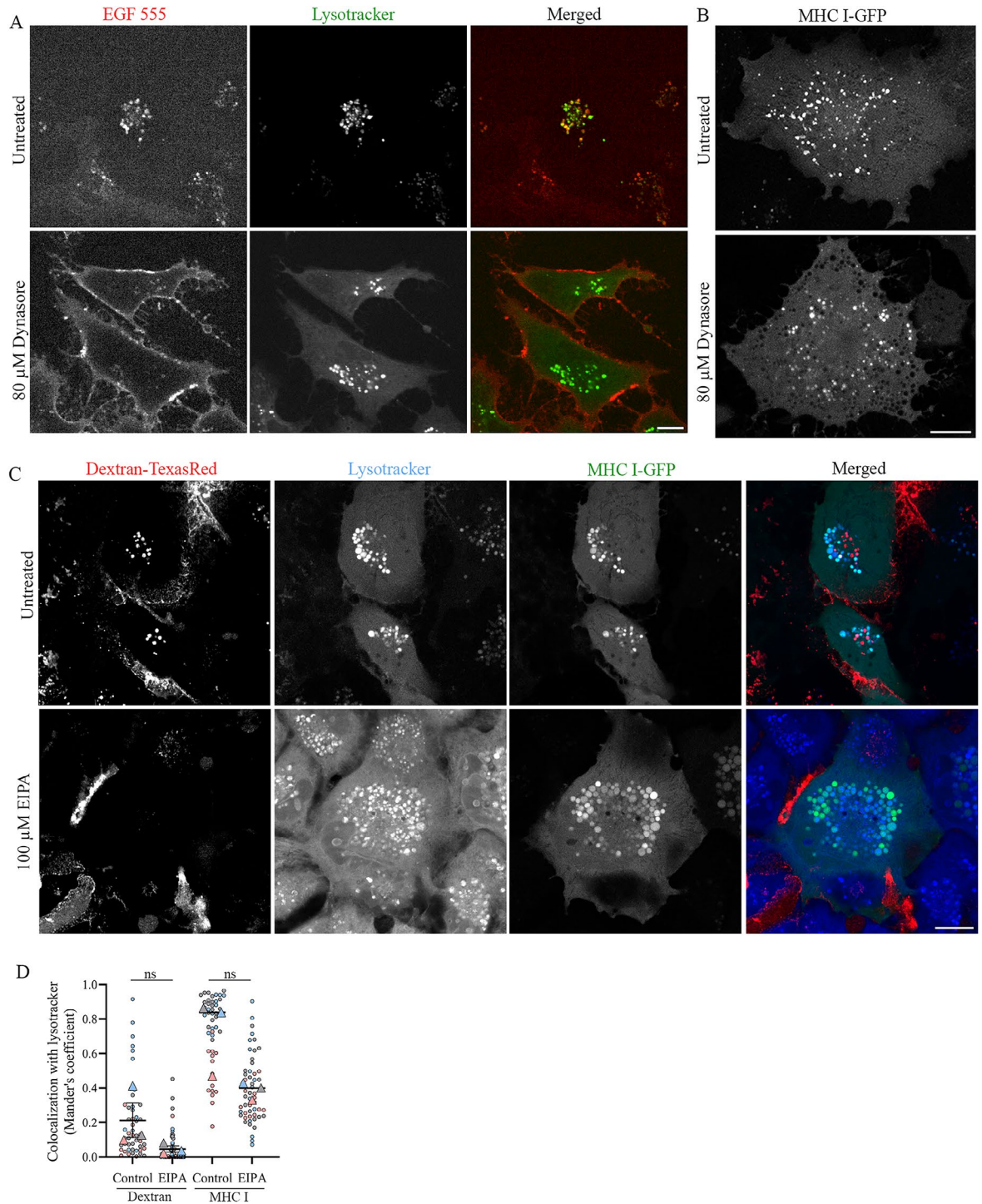
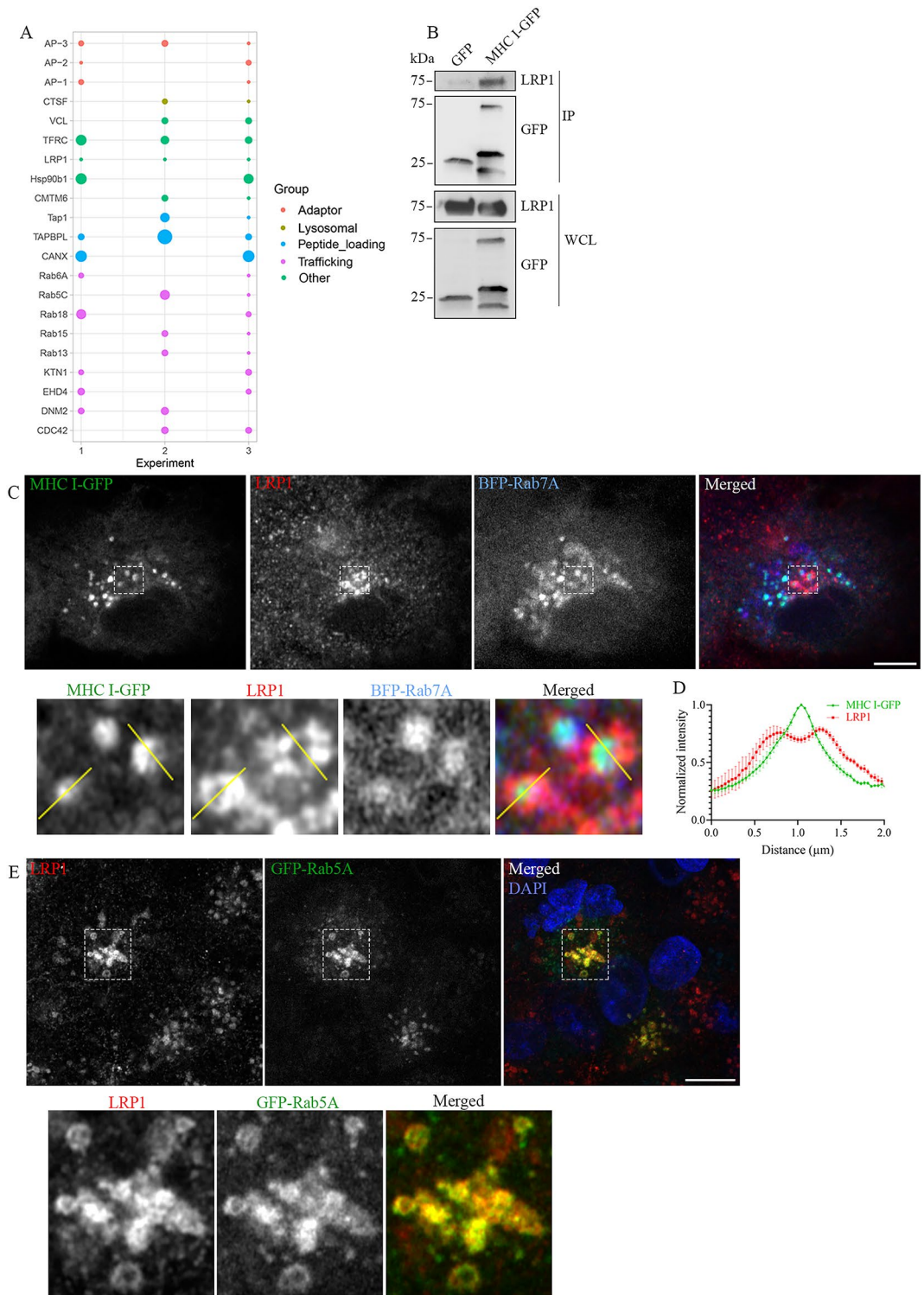


**Fig. 4.** Atlantic cod MHC I does not accumulate at the plasma membrane when endocytosis is blocked. **(A)** Representative image of ACL cells untreated or treated with 80  $\mu$ M Dynasore and incubated with 200 ng/ml EGF-Alexa555. Cells were stained using lysotracker green and imaged using an Olympus SpinSR SoRA microscope. Scale bar: 10  $\mu$ m. **(B)** Representative images of ACL cells transiently transfected with Atlantic cod MHC I-GFP, untreated or treated with 80  $\mu$ M Dynasore. Cells were imaged using a Zeiss LSM880 Fast AiryScan microscope. Scale bar: 10  $\mu$ m. **(C)** Representative image of ACL cells transiently transfected with Atlantic cod MHC IGFP, untreated or treated with 100  $\mu$ M EIPA and incubated with 0.1 mg/ml 70 kDa Dextran-TexasRed. Cells were stained using lysotracker blue and imaged using a Zeiss LSM880 Fast AiryScan microscope. Scale bar: 10  $\mu$ m. **(D)** The graph represents colocalization analysis between lysotracker blue and Dextran-TexasRed or MHC I-GFP in untreated or EIPA treated cells. Colocalization was analysed by calculating Manders' coefficient in ImageJ. Scatter plot shows the mean  $\pm$  SEM from three independent experiments, colour coded for each experimental repeat. Dots represent individual measurements and are colour coded according to experimental repeat.  $n > 48$  cells.



conducted on immunoprecipitated samples. Due to the lack of available antibodies recognizing Atlantic cod proteins, we were only able to confirm the interaction with LRP1 (Fig. 5B).

We next investigated whether MHC I and LRP1 colocalize to cMICs in ACL cells by immunofluorescence staining. ACL cells co-transfected with MHC I-GFP and BFP-Rab7A were fixed and immunostained with an antibody against LRP1. The results show that LRP1 is present on cMICs together with MHC I and Rab7A (Fig. 5C-D). Moreover, ACL cells transfected with GFP-Rab5A and immunostained with LRP1 reveal that LRP1 localizes to early endosomes (Fig. 5E), thus suggesting that LRP1 follows the endosomal pathway where it eventually colocalizes with MHC I. Immunofluorescence analysis was also performed on Atlantic cod primary hepatocytes and leukocytes transfected with MHC I-GFP. This further confirmed colocalization between MHC I-GFP and LRP1, but also revealed that MHC I and LRP1 can be present on distinct compartments that are closely interacting (Fig. 6A-D, Suppl. Figure 5B). As LRP1 is also present on early endosomes (Fig. 6E), the close

◀ **Fig. 5.** (A) Spectral counts of MHC I interactors obtained from ACL cells transiently transfected with MHC I-GFP and subjected to immunoprecipitation. The circles are proportional to the numbers of spectral counts. Values are from three independent experiments. Interactors in the list were only found in the cells transfected with MHC I-GFP, not in the control cells transfected with GFP and present in at least two of the three experimental repeats. Interactors are grouped into five different categories (Adaptor, Lysosomal, Peptide-loading, Trafficking, Other) and colour coded accordingly. For full list of values see Suppl. Table 1. (B) ACL cells were transiently transfected with either GFP or MHC I-GFP, lysed and subjected to immunoprecipitation with GFP magnetic agarose beads. Whole cell lysate (WCL) and immunoprecipitates (IP) were subjected to Western blot analysis using the indicated antibodies. Original full-size blots are presented in Supplementary Fig. 6. (C) Representative image of an ACL cell transiently co-transfected with MHC I-GFP and BFP-Rab7A, fixed and stained with antibody against LRP1. Cells were imaged using a Zeiss LSM880 Fast AiryScan microscope. Scale bar: 5  $\mu\text{m}$ . Magnification of boxed areas is shown below. The yellow lines in the magnified images illustrate regions selected for fluorescence intensity profile analysis. (D) The graph shows the normalized fluorescence intensity profiles relative to MHC I-GFP and LRP1 along the yellow lines as illustrated in the magnified images in (C), represented as mean  $\pm$  SEM from three independent experiments.  $n = 41$  vesicles from 14 cells. (E) Representative image of ACL cells transiently transfected with GFP-Rab5A, fixed, and stained with antibody against LRP1. Cells were imaged using a Zeiss LSM880 Fast AiryScan microscope. Scale bar: 10  $\mu\text{m}$ . Magnification of boxed area is shown below.

association between LRP1 and MHC I-positive endosomes may perhaps indicate transient fusion for exchange of antigens. Thus LRP1 is either present on cMICs or on compartments that are in close contact with the cMIC.

In summary, our results show that Atlantic cod MHC I localizes to a late endosomal compartment similar to mammalian MIIC and further suggest that cMIC could be a site for antigen loading in a similar manner.

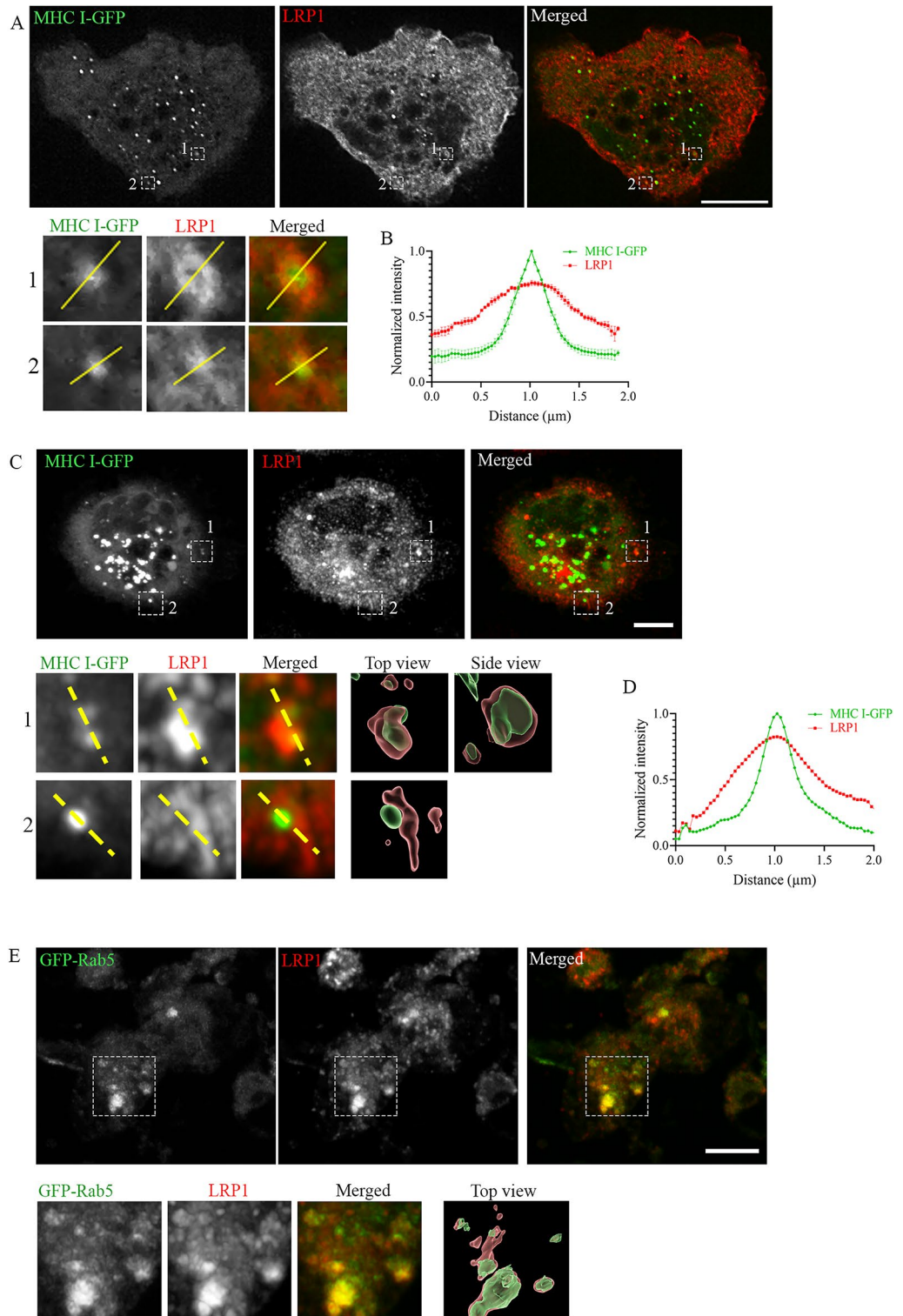
## Discussion

Along with the discovery of the MHC II-loss and the extreme expansion of MHC I gene copies, it was suggested that some Atlantic cod MHC I molecules may localize to endolysosomes replacing the MHC II pathway by presenting exogenous-peptides via cross-presentation<sup>9,63</sup>. This scenario would represent an evolutionary compensation for the absence of MHC II. Until now, there were no experimental evidence of such cross-presentation occurring in cod. In a recent study, however, we demonstrated that different Atlantic cod MHC I variants indeed localize to endolysosomes positive for Tapasin and Tap<sup>17</sup> which may be needed for exogenous peptide-loading of MHC I. To investigate this hypothesis further, we have here expanded our research characterizing this organelle, to determine if Atlantic cod MHC I positive compartment (cMIC) has the properties needed for proper peptide-loading.

From colocalization analysis using known endosomal markers, we found that cMICs in ACL cells are enriched with late endosomal markers such as Rab7A, Rab9, LIMP2, LAMP1 and CD63 rather than early and recycling markers such as Rab5, Rab11, Rab14, Rab22, HRS and SNX1 (Fig. 1, Suppl. Figures 1–2). Similar results were obtained in primary hepatocytes and leukocytes, where MHC I shows high degree of overlap with lysotracker and Rab7A (Fig. 2), confirming that cMIC is a late endosomal compartment. This is intriguing as in humans MHC I is primarily located to the cell-surface<sup>17,36</sup>, while MHC II resides on specialized late endosomes named MHC II compartments (MIICs). Most notably, in this work we reveal that cMICs have similarities with MIICs. Indeed, both compartments are characterized by acidic pH, the presence of proteases like cathepsins, and are positive for the late endosomal markers LAMP1 and CD63 (Figs. 1, 2 and 5, Suppl. Figure 1)<sup>3,18–24</sup>. Moreover, we detected MHC I in intraluminal vesicles inside large Rab7A-positive endosomes in primary leukocytes (Fig. 2H, J). Again, this is similar to what has been described for mammalian MHC II, which localizes to intraluminal vesicles of multivesicular bodies. MHC II then fuses with the limiting membrane of MVBs for interaction with the peptide-loading machinery for binding of exogenous peptides<sup>64–66</sup>. Hence, Atlantic cod MHC I might behave more like human MHC II, and its location to late acidic endosomes could allow for binding of exogenous peptide antigens. In line with this, we previously identified that Tapasin and other components of the peptide-loading complex (PLC) localize to the cMIC<sup>17</sup>.

Here, we provided an additional indication that peptide-loading may occur in this compartment, by identifying LRP1 (also known as CD91) and Hsp90b1 (also known as Grp94) as interactors of MHC I in Atlantic cod (Fig. 5A–B). These proteins are known to work in cross-presentation in humans, where Hsp90b1 binds exogenous peptides from the cell-surface<sup>55</sup>, and the cell-surface receptor LRP1 binds and internalize the Hsp90b1-peptide complex. Once internalized, LRP1 and Hsp90b1 co-localize with MHC I on endosomes where exogenous peptides can be cross-presented<sup>55</sup>. Therefore, the interaction between MHC I, Hsp90b1 and LRP1 in Atlantic cod, and the localization of LRP1 to cMICs (Figs. 5 and 6) further suggest that cMIC is a site for peptide cross-presentation. As our data suggest that Atlantic cod MHC I does not enter the endosomes from the plasma membrane (Fig. 4), but it still able to meet LRP1 in the cMIC, it is tempting to speculate that MHC I could be transported to the endolysosomes directly from the trans-Golgi network like MHC II in mammals.

Interestingly, we also identified the lysosomal protease cathepsin F (CATF) as an interactor of Atlantic cod MHC I (Fig. 5A). CATF is part of the cathepsin family, whose members comprise the most abundant proteases in the endolysosomal system<sup>67</sup>. Cathepsins participate in many proteolytic events, contributing to protein turnover, but also to antigen production and proper MHC II loading<sup>67,68</sup>. The activity of cathepsins are tightly regulated, and low pH is required for both their activation and their ability to bind substrate<sup>67</sup>. Interestingly, CATF has been shown to be involved in degradation of the Ii for proper peptide loading of MHC II<sup>52,54</sup>. Thus, the fact that in Atlantic cod MHC I co-immunoprecipitates with CATF not only indicates that the cMIC is a late endosomal/



lysosomal compartment, but opens up for the possibility that CATF could aid in the generation of exogenous peptide fragments for MHC I loading.

During cross-presentation in mammalian cells, MHC I relocates from recycling endosomes to bacteria-containing phagosomes<sup>32,69</sup>. We did not detect any significant relocation of MHC I in Atlantic cod upon infection with the facultative intracellular bacterium *Francisella noatunensis subsp. noatunensis* (*Fnn*). However, we proved that *Fnn* reaches and escapes cMICs (Fig. 3), in line with existing literature reporting that *Fnn* escapes degradation by exiting endosomes, similarly to the human pathogen *Francisella tularensis*<sup>34,35</sup>. This indicates that MHC I is together with endocytosed material, further supporting the hypothesis of cross-presentation. Indeed, the fact that phagocytosed bacteria are present in MHC I-positive compartments in Atlantic cod suggests a similar response as in humans during cross-presentation<sup>32,69–71</sup>.

◀ **Fig. 6.** Atlantic cod MHC I co-localize with LRP1 in Atlantic cod hepatocytes and leukocytes. **(A)** Representative image of an Atlantic cod primary hepatocyte transiently transfected with MHC IGFP, fixed, and stained with antibody against LRP1. Cells were imaged using a Zeiss LSM880 Fast AiryScan microscope. Scale bar: 10  $\mu\text{m}$ . Magnification of boxed areas are shown below. The yellow lines in the magnified images illustrate regions selected for fluorescence intensity profile analysis. **(B)** The graph shows the normalized fluorescence intensity profiles relative to MHC IGFP and LRP1 represented as mean  $\pm$  SEM ( $n = 164$  vesicles from 21 cells from three fish specimens). **(C)** Representative image of an Atlantic cod primary leukocyte transiently transfected with MHC IGFP, fixed, and stained with antibody against LRP1. Cells were imaged using a Zeiss LSM880 Fast AiryScan microscope. Scale bar: 5  $\mu\text{m}$ . Magnification of boxed areas are shown below. The yellow lines in the magnified images illustrate regions selected for fluorescence intensity profile analysis. **(D)** Imaparis isosurface 3D rendering of the boxed areas are shown to the right. **(E)** The graph shows the normalized fluorescence intensity profiles relative to MHC I-GFP and LRP1 represented as mean ( $n = 81$  vesicles from 11 cells from one fish). **(F)** Representative image of Atlantic cod primary leukocytes transiently transfected with GFP-Rab5, fixed, and stained with antibody against LRP1. Cells were imaged using a Zeiss LSM880 Fast AiryScan microscope. Scale bar: 5  $\mu\text{m}$ . Magnification of the boxed area is shown below. Imaparis isosurface 3D rendering of the boxed area is shown to the right.

How does MHC I traffic to the cMIC? In mammalian cross-presentation, MHC I can enter late endosomes either from the cell-surface by endocytosis<sup>40</sup>, or by transport from the endoplasmic reticulum through the association with Ii<sup>41</sup>. As Atlantic cod lacks Ii, we investigated if MHC I is delivered to cMICs following internalization from the cell surface. The results show no accumulation of MHC I at the cell surface in either Dynasore or EIPA treated cells (Fig. 4), indicating that Atlantic cod MHC I does not traffic to the cMIC from the plasma membrane by dynamin-dependent mechanisms, nor by macropinocytosis. We cannot exclude that an alternative endocytic mechanism is used by Atlantic cod to internalize MHC I from the plasma membrane, as additional endocytic mechanisms have been reported to occur in mammals<sup>37,38,72</sup>. On the other hand, MHC I transport to the cMIC could follow a direct rather than a recycling route, such as for the non-canonical cross-presentation pathway<sup>69,73</sup>. In this pathway, MHC I traffics directly from the ER-Golgi intermediate compartment (ERGIC) to the late endosomal/phagosomal compartments<sup>69,73</sup>. However, our recent results showing that the introduction of mutations or deletions in the cytoplasmic tail of Atlantic cod MHC I does not alter MHC I localization to endolysosomes, indicate that MHC I transport to endolysosomes is independent of sorting signals<sup>17</sup>. Therefore, it is likely that Atlantic cod MHC I transport to the endosomal pathway depend on an unknown chaperone.

In sum, our findings demonstrate that cMIC is a late endosomal compartment with many similar characteristics as the mammalian MIIC. Atlantic cod is not a model organism and therefore there are no available tools to assess antigen presentation ability. However, our data suggest the possibility of exogenous antigen-binding for Atlantic cod MHC I as a compensatory or evolutionary alternative mechanism in the absence of MHC II and associated molecules.

## Materials and methods

### Cell culture

ACL cells<sup>27</sup> were grown in IMDM (Gibco) supplemented with 10% FCS (BioWest), 2% Hepes buffer solution (Gibco), 1% L-glutamine (Gibco), 1% Non-Essential Amino Acids solution (Gibco) and 0.1% penicillin and streptomycin (Gibco). Cells were maintained in a 4.5% CO<sub>2</sub> atmosphere at 15 °C.

### Sampling of fish

Atlantic cod were collected at 95–100 m depth in the inner Oslofjord (N 59° 48.729, E 010° 32.952) using demersal trawl. Immediately following retrieval, cod were terminated by an acute blow to the head. Individuals were then weighed and the length measured before blood was withdrawn and hepatocytes and leukocytes isolated as described below. Samples were taken *post-mortem* and no scientific experiments have been performed on live animals. Personnel involved had ethical certification.

### Isolation of hepatocytes and leukocytes from Atlantic Cod

Hepatocytes were isolated from Atlantic cod immediately after termination by two-step perfusion as described before<sup>74</sup>. Shortly, fish were opened from the ventral side. A cannula was introduced in the largest and most available hepatic vein and the vena cava was cut, allowing perfusion of at least one lobe. Isolation of hepatocytes was done using perfusion buffer (NaCl 122 mM, KCl 4.8 mM, MgSO<sub>4</sub> 1.2 mM, Na<sub>2</sub>HPO<sub>4</sub> 11 mM, NaH<sub>2</sub>PO<sub>4</sub> 3.8 mM and NaHCO<sub>3</sub> 3.7 mM adjusted to pH 7.5) supplemented with different reagents. The first round of perfusion was done using perfusion buffer supplemented with ethylene glycol tetra acetic acid (EGTA, 26  $\mu\text{M}$ ). Perfusion was done for approximately 10–15 min (10 ml/min, adjusted with a speed regulator on the perfusion tube) until all blood was replaced with buffer. The liver was then perfused a second time for 10–15 min (10 ml/min) with perfusion buffer supplemented with 0.3 g/l collagenase type IV (Sigma Aldrich) and 2 mM CaCl<sub>2</sub> preheated to 37 °C to obtain maximal collagenase activity. After this, the perfused part of the liver was removed and suspended in ice-cold perfusion buffer supplemented with bovine serum albumin (BSA, 15 mM, Sigma Aldrich). The small liver-pieces were filtered through a 200  $\mu\text{m}$  cell strainer, followed by a second filtration through a 100  $\mu\text{m}$  cell strainer (pluriStrainer<sup>®</sup>, from Pluri Select). The cell suspension was then centrifuged three times at 50  $\times$  g. After the first centrifugation, the pellet was resuspended in ice-cold perfusion buffer containing BSA, and after the second centrifugation, the pellet was resuspended in Dulbecco's Modified Eagle Medium

(DMEM; Lonza, BioWhittaker) containing 5% fetal calf serum (FCS, BioWest), 2 mM L-glutamine (Gibco), 100 U/ml penicillin (Gibco), 100 µg/ml streptomycin (Gibco), 0.25 µg/ml Amphotericin B (Sigma Aldrich). After the last centrifugation, the pellet was resuspended in DMEM also containing 0.01 M HEPES (Gibco). Resuspended cells were transferred to T25 culture flasks (VWR) and kept temporarily at 4 °C until arriving back at the lab where they were maintained at 4.5% CO<sub>2</sub> atmosphere at 10 °C. Hepatocyte viability and cell density was determined using trypan blue (Sigma Aldrich) and a Bürker-Türk counting chamber. Samples with at least 70% viable hepatocytes were used for transfection. Hepatocytes were transfected the same day as isolation.

Leukocytes were isolated from Atlantic cod blood and head-kidney immediately after termination as previously described<sup>75</sup>. Briefly, peripheral blood (1–2 ml) was extracted from the caudal vein using a heparinized syringe (cannula 0.6 mm). The extracted blood was diluted 1:1.5 using cell culture medium (CCM) (Leibovitz L-15 (Sigma Aldrich) supplemented with 5% FCS (BioWest), 36 mM NaCl (380 mOsm), 10 U/ml Heparin (Panpharma Nordic AS), 0.29 mg/ml L-glutamine (Lonza), 100 U/ml Penicillin (Gibco), 100 µg/ml Streptomycin (Gibco), 0.25 µg/ml Amphotericin B (Sigma Aldrich) and 0.01 M HEPES (Gibco)) and stored on ice. Head-kidney were extracted from Atlantic cod and filtered through a 100 µm cell strainer (pluriStrainer®, from Pluri Select) using 1 ml ice cold CCM. The strainer was flushed with additional 4 ml of CCM. Leukocytes were isolated from the peripheral blood and head-kidney cell suspension by centrifugation on a discontinuous two-layered Percoll gradient (Cytiva) prepared in a 15 ml falcon tube with 2.5 ml 1.070 g/l bottom layer and a 2.0 ml 1.050 g/l top layer. Centrifugation was done using a swing-out rotor at 400 × g and 10 °C for 40 min. Leukocytes were collected from the interface between the 1.070 and 1.050 g/l layer and diluted 2x in CCM. Cells were centrifuged at 400 × g and 10 °C for 10 min and the pellet resuspended in 5 ml ice cold CCM. Isolated leukocytes were transferred to T25 culture flasks (VWR) and kept temporarily at 4 °C until arriving back at the lab where they were maintained at 4.5% CO<sub>2</sub> atmosphere at 10 °C. Leukocytes were kept overnight to properly adhere, and only adherent cells were used for downstream transfection.

### Constructs

pEGFP-N3 and mCherry-pcDNA3.1-C-HA constructs containing Atlantic cod MHC I variant 1 have been described before<sup>17</sup>. The rest of the constructs used in this study are of mammalian origin. Before expressing the mammalian constructs in cells derived from Atlantic cod, alignment analysis between mammalian and Atlantic cod endosomal and lysosomal markers were performed using their overall sequence (Suppl. Table 2) and phylogenetic clustering (Suppl. Figure 4). The analysis demonstrates high degree of conservation. BFP-Rab7A and RFP-Rab9 were kind gifts from Yael Elbaz-Alon (Weizmann Institute of Science, Israel)<sup>76</sup> and Stefan Hönig (University of Cologne, Germany)<sup>77</sup>, respectively. mApple-Rab7A (Addgene plasmid #54945; <http://n2t.net/addgene:54945>; RRID: Addgene\_54945) and mApple-Rab11A (Addgene plasmid #54942; <http://n2t.net/addgene:54942>; RRID: Addgene\_54942) were gifts from Michael Davidson. mCherry-Rab5A has been described before<sup>78</sup>. GFP-Rab14 was a kind gift from Ole Landsverk, GFP-Rab22 was purchased from Addgene (plasmid #49600). HRSYFP has been described before<sup>79</sup>. RFP-SNX1 was a kind gift of Peter Cullen (University of Bristol, UK), LAMP1-mGFP was a gift from Esteban Dell'Angelica (Addgene plasmid #34831; <http://n2t.net/addgene:34831>; RRID: Addgene\_34831)<sup>80</sup>, CD63-GFP has been described before<sup>81</sup>. GFP-Rab5A was a kind gift of Cecilia Bucci (University of Salento, Italy). For the construction of mCherry-LIMP2, the coding sequence of LIMP2 was amplified by polymerase chain reaction (PCR) using the following primers: LIMP2-f 5'-AGAGA GCGGCCGCAATGGCCGATGCTGCTTCTA-3'; LIMP2-r 5'-AGAGATCTAGATTAGGTCCGTATGAGGG GTG-3'; containing a NotI restriction site and a XbaI restriction site, respectively. LIMP2 fragments cut with NotI/XbaI were then cloned into pcDNA 3.1-mCherry plasmid<sup>82</sup> cut with NotI and XbaI. The construct was sequenced to exclude the presence of Taq polymerase mistakes.

### Sequence alignments and phylogenetic tree

Sequences of human molecular markers were obtained from <https://vertebrate.genenames.org> through their link to Refseq gene models. Canonical transcripts were downloaded through NCBI. For Atlantic cod molecular markers were obtained through gene name searches <https://www.ncbi.nlm.nih.gov/data-hub/gene/taxon/8049/>. In addition, a small set of protein coding sequences from other species were downloaded from GenBank to be included in a multiple protein sequence alignment. MEGA7 was used to curate Atlantic cod and human transcript sequences and alignments done using muscle. Pairwise p-distances were calculated using the protein sequences in MEGA7. The p-distance reflects the proportion of amino acid sites at which two sequences compared are different. Using the translated protein alignment, additional protein sequences were added and re-aligned using muscle. A simple unrooted neighbour-joining tree with Poisson distribution and 500 bootstrap replicates was generated to investigate if the annotated Atlantic cod gene models likely share ancestry with the annotated human gene models. All annotations clustered together with their human orthologs.

### Antibodies and reagents

Primary antibodies used for western blot (WB) and immunofluorescence (IF) analysis include antiLRP1 (Invitrogen, SA0290, IF 1:100, WB 1:200) and anti-GFP (Abcam, ab6556, WB 1:1000). Alexa Fluor secondary antibodies (Invitrogen) used for IF were diluted to 1:200 and secondary antibodies conjugated to horseradish peroxidase used for immunoblotting studies (GE Healthcare) were diluted 1:5000. LysoTracker™ Red DND-99 (Invitrogen), LysoTracker™ Green DND-26 (Invitrogen) and LysoTracker™ Blue DND-22 (Invitrogen) were used at a final concentration of 50 nM, 1 µM and 2 µM, respectively. Before imaging, cells were incubated with red, green or blue LysoTracker for 15 min. EGF-Alexa555 (from Invitrogen) was used at a final concentration of 200 ng/ml and imaged after 15 min uptake. Dynasore<sup>42</sup> (Sigma Aldrich) was used at a final concentration of 80 µM for 1 h before imaging. 70 kDa Dextran-TexasRed (Molecular Probes) was used at a final concentration of

0.1 mg/ml and imaged after 1 h uptake. EIPA<sup>47,48</sup> (Sigma Aldrich) was used at a final concentration of 100  $\mu$ M for 2 h before imaging.

### Transfection

Amaya nucleofector 2b (Lonza) was used to transfect ACL cells and primary cells using the program X-005. For each transfection-reaction of the ACL cells, 1/6 of a confluent T75 flask (VWR) was used while for the primary cells,  $10^6$  cells were used. For each transfection-reaction, 2  $\mu$ g DNA were used. Both ACL cells and primary cells were seeded onto 35-mm-diameter imaging dishes with glass bottom (MatTek) coated with 20  $\mu$ g/ $\mu$ L fibronectin (Sigma Aldrich). Cells were transfected for at least 4 days (for single transfection) or 7 days (for double/triple transfections) prior to downstream experiments.

### Immunoblotting

Lysis of cells was done using a lysis-buffer containing 125 mM K-acetate, 25 mM Hepes, 5 mM EGTA, and 2.5 mM Mg-acetate, pH 7.2, complemented with 0.5% NP-40, protease inhibitor cocktail (Sigma Aldrich), and DTT (Sigma Aldrich). Lysates were run on SDS-PAGE, blotted onto polyvinylidene fluoride (PVDF) membranes (Millipore), then incubated with primary antibodies in 2% blotting grade non-fat dry milk (BioRad). After overnight incubation with primary antibodies, the membranes were incubated with secondary antibodies conjugated to horseradish peroxidase (HRP) (GE Healthcare). Chemiluminescence was detected using ECL Prime Western Blotting Detection (GE Healthcare) and a ChemiDoc imaging system from BioRad.

### Co-immunoprecipitation

For co-immunoprecipitation experiments, the GFP-Trap<sup>+</sup> MA (Chromotek)-system was used. Cells were transiently transfected with GFP-fusion proteins, then lysed in lysis buffer containing 10 mM Tris-HCl pH 7.5, 150 mM NaCl, 0.5 mM EDTA, and 0.1% NP-40. Lysates were incubated for 1 h at 4 °C together with magnetic beads coupled with anti-GFP. Immunoprecipitated samples together with their respective total lysates were run on SDS-PAGE and analysed by western blotting.

### LC-MS/MS, protein identification and data analysis

The supernatants from the co-immunoprecipitated samples were removed, and the protein-bound beads were dissolved in 50  $\mu$ l 50mM ammonium bicarbonate. The proteins were reduced by adding 10 mM DTT and incubating at 30 °C for 30 min, and then alkylated by adding 25 mM iodoacetamide and incubating at 23 °C for 60 min in the dark. The reaction was quenched by incubating with 30 mM DTT at 30 °C for 30 min. The samples were then digested with 2  $\mu$ g trypsin Trypsin Gold (Promega) at 37 °C overnight. The next day the digestion was stopped by adding 1% formic acid and the peptides were cleaned by solid-phase extraction (SPE) using a Ziptip-C18 (Millipore). The digested samples were analyzed using a nanoElute LC system coupled to a timsTOF Pro mass spectrometer (Bruker Daltonics). The peptides were separated by liquid chromatography with a Aurora 25 column (C18, 1.5  $\mu$ m beads, 75  $\mu$ m inner diameter, 25 cm length; IonOptics) using a flow rate of 200 nl/min with 0.1% formic acid (solvent A) and 0.1% formic acid in acetonitrile (solvent B). A 30-minute gradient was used, starting from 2% solvent B to 35% at a column temperature of 50 °C. MS acquisition was performed in DDA-PASEF mode. Precursors for data-dependent acquisition were fragmented with an ion mobility-dependent collision energy, which was linearly increased from 20 to 59 eV.

The LC/MS data were searched against the NCBI database of Atlantic cod (45,162 entries) using Mascot (Matrix Science, version 2.7.0.1). Scaffold (Proteome Software Inc., Scaffold version 5.1.2) was used to validate MS/MS based peptide and protein identifications. Peptide identifications were accepted if they achieved an FDR less than 1.0% by the Percolator posterior error probability calculation. Protein identifications were accepted if they achieved an FDR less than 1%. For label-free quantification using spectral counts, a t-test was applied with significance level  $p < 0.05$ , using normalization and average TIC as quantitative method.

### Bacterial strain and growth conditions

*F. noatunensis* subsp. *Noatunensis* (*Fnn*) strain NCIMB14265 isolated from diseased Atlantic cod (*Gadus morhua*) and transformed with the mCherry-expressing plasmid pKK289Km/mCherry (*Fnn*-mCherry)<sup>83</sup> was kindly provided by Hanne C. Winther-Larsen from the Department of Pharmacy, University of Oslo, Norway. *Fnn* was kept at -80 °C for long-term storage in BD Bacto Eugon broth (BD Diagnostic Systems) supplemented with 20% glycerol (Sigma Aldrich). Prior to experiments, bacteria were plated onto Eugon blood agar (EBA) plates (30.4 g/l BD Bacto Eugon, 15 g/l agar and 5% bovin blood, from Håttunlab), supplemented with 25  $\mu$ g/ml kanamycin (Sigma Aldrich), incubated at 20 °C. 4 days prior to infection, *Fnn* was inoculated in Eugon broth supplemented with 2 mM FeCl<sub>3</sub> (Sigma Aldrich) and 25  $\mu$ g/ml kanamycin (Sigma Aldrich), incubated at 20 °C with shaking at 150 rpm.

### Infection of ACL cells

Transfected ACL cells were seeded onto 24-well plate with glass bottom (MatTek) coated with 20  $\mu$ g/ $\mu$ l fibronectin (Sigma Aldrich). Cells were washed 3 times in PBS, then incubated in IMDM medium (Gibco) without antibiotic and with heat-inactivated FCS (heat to 56 °C for 30 min). Day 7 after transfection, cells were infected with *Fnn*-mCherry growing in their exponential phase ( $OD_{600} = 1.5-1.8$ ) and diluted to  $OD_{600} = 1$  in IMDM medium without antibiotics and with heat-inactivated FCS. After adding bacteria to the ACL cells, the plates were centrifuged at 500  $\times$  g for 5 min to synchronize bacterial uptake. Colony forming units (cfu) was determined by spreading tenfold dilutions on EBA plates. Growth of pure colonies was counted after 7 days. ACL cells were infected for 6 h with multiplicity of infection (MOI) of 2500 and kept at 15 °C, 4.5% CO<sub>2</sub>.

### Immunofluorescence

Cells were fixed in 3% paraformaldehyde (PFA) for 20 min, quenched 10 min in 50 mM NH<sub>4</sub>Cl, then permeabilized with 0.25% saponin in 1x PBS for 5 min. Following this, cells were incubated 20 min with primary antibody diluted in 1x PBS, washed three times in 1x PBS, then incubated 20 min with Alexa Fluor 647-conjugated secondary antibody (Invitrogen) in 1x PBS for 20 min.

### Live-cell microscopy

During live-cell imaging, cells were kept at room temperature with 4.5% CO<sub>2</sub>. Imaging was done using a Zeiss LSM880 microscope equipped with a 63 × oil Plan Apo NA 1 objective or an Olympus SpinSR SoRA spinning disk confocal using a 60 × Planon NA 1.42 objective.

### Imaging processing and analysis

Image analysis and processing was done using ImageJ (National Institutes of Health) and Adobe Photoshop (Adobe Systems). Graphs and volcano plot were generated using the software GraphPad Prism 9 (GraphPad Software Inc., <https://www.graphpad.com>). Colocalization was analysed by pixel-based analysis using Mander's coefficient with the JACoP plugin in ImageJ<sup>84</sup>. Imaris software was used to generate isosurface 3D reconstructions. Ggplot was generated in R illustrating the mass spectrometry data. Fluorescence intensity profile analysis were obtained using the plot profile function in ImageJ. Statistical analysis was done using two-tailed paired Student t-test in Excel (Microsoft). In the figures, statistical significance is indicated as follows: ns > 0.05, \**p* < 0.05, \*\**p* < 0.01.

### MHC I expression analysis

All RefSeq gene models from the Atlantic cod genome assembly gadmor3 GCF\_902167405.1 were subjected to a TblastN search using teleost reference MHCI sequences from Grimholt et al. as queries<sup>85</sup> and BLAST+/2.14<sup>86</sup>. All reported transcripts were translated to protein and aligned together with the reference sequences using CLUSTALW and Mega<sup>787</sup>. Only transcripts clustering together with MHCI U and Z lineages were selected for further analysis. Their corresponding LOC gene identifiers were obtained from the GCF\_902167405.1 GTF file. RNA expression data from 10 different Atlantic cod tissues was downloaded from SRA: Ovary SRR2045415, Brain SRR2045416, Gills SRR2045417, Heart SRR2045418, Muscle SRR2045419, Liver SRR2045420, Kidney SRR2045421, Bones SRR2045422, Intestine SRR2045423, and Testis SRR2045424. The raw sequence data was mapped towards gadmor3 using STAR/2.7.10b<sup>88</sup> using default parameters and quantMode GeneCounts. The resulting unstranded counts were merged into a count matrix and analysed using Rstudio (R version 4.3.2). The matrix was filtered by expression using edgeR<sup>89</sup> FilterByExprs function prior to any data conversion and plotting. As there are no replicates, and the main goal is to determine present or absent MHCI expression in different tissues, the collective data was first converted to log<sub>2</sub> transformed counts per million and plotted using the base boxplot function. Subsequently, using DESeq2<sup>90</sup>, the log<sub>2</sub> transformed counts were plotted per predicted MHCI gene in the annotation using the plotCounts function. Count matrix, code and plots is available here: <https://doi.org/10.6084/m9.figshare.24973524>.

### Data availability

RNA sequences for MHC I expression analyses are available in the Sequence Read Archive repository, under the following accession: Ovary SRR2045415, Brain SRR2045416, Gills SRR2045417, Heart SRR2045418, Muscle SRR2045419, Liver SRR2045420, Kidney SRR2045421, Bones SRR2045422, Intestine SRR2045423, and Testis SRR2045424. Code for mapping, subsequent count matrix, code for MHC I expression analysis, and results are available at Figshare: <https://doi.org/10.6084/m9.figshare.24973524>. Accession numbers used for phylogenetic tree analyses are available in supplementary Table 3. All alignments are available at Figshare: <https://doi.org/10.6084/m9.figshare.24973524>. The mass spectrometry proteomics data have been deposited to the ProteomeXchange Consortium via the PRIDE partner repository<sup>91</sup> with the dataset identifier PXD050180 (<http://www.ebi.ac.uk/pride>).

Received: 6 February 2024; Accepted: 11 October 2024

Published online: 25 October 2024

### References

- Litman, G. W., Rast, J. P. & Fugmann, S. D. The origins of vertebrate adaptive immunity. *Nat. Rev. Immunol.* **10**, 543–553 (2010).
- Flajnik, M. F. & Kasahara, M. Origin and evolution of the adaptive immune system: genetic events and selective pressures. *Nat. Rev. Genet.* **11**, 47–59 (2010).
- Neefjes, J., Jongstra, M. L. M., Paul, P. & Bakke, O. Towards a systems understanding of MHC class I and MHC class II antigen presentation. *Nat. Rev. Immunol.* **11**, 823–836 (2011).
- Embgenbroich, M. & Burgdorf, S. Current concepts of Antigen Cross-presentation. *Front. Immunol.* **9**, 1643 (2018).
- Colbert, J. D., Cruz, F. M. & Rock, K. L. Cross-presentation of exogenous antigens on MHC I molecules. *Curr. Opin. Immunol.* **64**, 1–8 (2020).
- Mantegazza, A. R. et al. NADPH oxidase controls phagosomal pH and antigen cross-presentation in human dendritic cells. *Blood* **112**, 4712–4722 (2008).
- Blander, J. M., Yee Mon, K. J., Jha, A. & Roycroft, D. Chapter Two—The show and tell of cross-presentation. In *Advances in Immunology*, Vol. 159 (eds F.W. Alt & K.M. Murphy) 33–114 (Academic Press, 2023).
- Flajnik, M. F. A cold-blooded view of adaptive immunity. *Nat. Rev. Immunol.* **18**, 438–453 (2018).
- Star, B. et al. The genome sequence of Atlantic Cod reveals a unique immune system. *Nature* **477**, 207–210 (2011).
- Haase, D. et al. Absence of major histocompatibility complex class II mediated immunity in pipefish, *Syngnathus typhle*: evidence from deep transcriptome sequencing. *Biol. Lett.* **9**, 20130044 (2013).

11. Dubin, A., Jørgensen, T. E., Moum, T., Johansen, S. D. & Jakt, L. M. Complete loss of the MHC II pathway in an anglerfish, *Lophius piscatorius*. *Biol. Lett.* **15**, 20190594 (2019).
12. Roth, O. et al. Evolution of male pregnancy associated with remodeling of canonical vertebrate immunity in seahorses and pipefishes. *Proc. Natl. Acad. Sci.* **117**, 9431–9439 (2020).
13. Swann, J. B., Holland, S. J., Petersen, M., Pietsch, T. W. & Boehm, T. The immunogenetics of sexual parasitism. *Science* **369**, 1608–1615 (2020).
14. Malmström, M. et al. Evolution of the immune system influences speciation rates in teleost fishes. *Nat. Genet.* **48**, 1204–1210 (2016).
15. Tørresen, O. K. et al. An improved genome assembly uncovers prolific tandem repeats in Atlantic Cod. *BMC Genom.* **18**, 95 (2017).
16. Tørresen, O. K. et al. Genomic architecture of haddock (*Melanogrammus aeglefinus*) shows expansions of innate immune genes and short tandem repeats. *BMC Genom.* **19**, 240 (2018).
17. Bjørnstad, S. A. et al. Atlantic Cod (*Gadus morhua*) MHC I localizes to endolysosomal compartments independently of cytosolic sorting signals. *Front. Cell. Dev. Biol.* **11**, 1050323 (2023).
18. Pieters, J. MHC class II compartments: specialized organelles of the endocytic pathway in antigen presenting cells. *Biol. Chem.* **378**, 751–758 (1997).
19. Rocha, N. & Neeffes, J. MHC class II molecules on the move for successful antigen presentation. *Embo J.* **27**, 1–5 (2008).
20. Peters, P. J., Neeffes, J. J., Oorschot, V., Ploegh, H. L. & Geuze, H. J. Segregation of MHC class II molecules from MHC class I molecules in the golgi complex for transport to lysosomal compartments. *Nature* **349**, 669–676 (1991).
21. Hsing, L. C. & Rudensky, A. Y. The lysosomal cysteine proteases in MHC class II antigen presentation. *Immunol. Rev.* **207**, 229–241 (2005).
22. Kleijmeer, M. J., Raposo, G. & Geuze, H. J. Characterization of MHC class II compartments by immunoelectron microscopy. *Methods* **10**, 191–207 (1996).
23. Tulp, A., Verwoerd, D., Dobberstein, B., Ploegh, H. L. & Pieters, J. Isolation and characterization of the intracellular MHC class II compartment. *Nature* **369**, 120–126 (1994).
24. Honey, K. & Rudensky, A. Y. Lysosomal cysteine proteases regulate antigen presentation. *Nat. Rev. Immunol.* **3**, 472–482 (2003).
25. Subramanian, M. et al. An AXL/LRP-1/RANBP9 complex mediates DC efferocytosis and antigen cross-presentation in vivo. *J. Clin. Investig.* **124**, 1296–1308 (2014).
26. Singh-Jasuja, H. et al. Cross-presentation of glycoprotein 96-associated antigens on major histocompatibility complex class I molecules requires receptor-mediated endocytosis. *J. Exp. Med.* **191**, 1965–1974 (2000).
27. Jensen, I. et al. Establishing a cell line from Atlantic Cod as a novel tool for in vitro studies. *Fish Shellfish Immunol.* **34**, 199–208 (2013).
28. Datsomor, A. K., Wilberg, R., Torgersen, J. S., Sandve, S. R. & Harvey, T. N. Efficient transfection of Atlantic salmon primary hepatocyte cells for functional assays and gene editing. *G3 Genes Genomes Genet.* **13**, jkad039 (2023).
29. van de Weijer, M. L., Luteijn, R. D. & Wiertz, E. J. H. J. viral immune evasion: lessons in MHC class I antigen presentation. *Semin. Immunol.* **27**, 125–137 (2015).
30. Neeffes, J. CIIV, MHC and other compartments for MHC class II loading. *Eur. J. Immunol.* **29**, 1421–1425 (1999).
31. Stern, L. J., Potoличchio, I. & Santambrogio, L. MHC class II compartment subtypes: structure and function. *Curr. Opin. Immunol.* **18**, 64–69 (2006).
32. Nair-Gupta, P. et al. TLR signals induce phagosomal MHC-I delivery from the endosomal recycling compartment to allow cross-presentation. *Cell* **158**, 506–521 (2014).
33. Birkbeck, T. H., Feist, S. W. & Verner-Jeffreys, D. W. Francisella infections in fish and shellfish. *J. Fish. Dis.* **34**, 173–187 (2011).
34. Brodmann, M., Dreier, R. F., Broz, P. & Basler, M. Francisella requires dynamic type VI secretion system and ClpB to deliver effectors for phagosomal escape. *Nat. Commun.* **8**, 15853 (2017).
35. Bakkemo, K. R. et al. Intracellular localisation and innate immune responses following *Francisella noatunensis* infection of Atlantic Cod (*Gadus morhua*) macrophages. *Fish. Shellfish Immunol.* **31**, 993–1004 (2011).
36. Wälchli, S. et al. Invariant chain as a vehicle to load antigenic peptides on human MHC class I for cytotoxic T-cell activation. *Eur. J. Immunol.* **44**, 774–784 (2014).
37. Adiko, A. C., Babbod, J., Gutiérrez-Martínez, E., Guermónprez, P. & Saveanu, L. Intracellular transport routes for MHC I and their relevance for antigen cross-presentation. *Front. Immunol.* **6**, 335 (2015).
38. Montealegre, S. & van Endert, P. M. Endocytic recycling of MHC class I molecules in non-professional antigen presenting and dendritic cells. *Front. Immunol.* **9**, 3098 (2018).
39. Joffre, O. P., Segura, E., Savina, A. & Amigorena, S. Cross-presentation by dendritic cells. *Nat. Rev. Immunol.* **12**, 557–569 (2012).
40. Lizée, G. et al. Control of dendritic cell cross-presentation by the major histocompatibility complex class I cytoplasmic domain. *Nat. Immunol.* **4**, 1065–1073 (2003).
41. Basha, G. et al. A CD74-dependent MHC class I endolysosomal cross-presentation pathway. *Nat. Immunol.* **13**, 237–245 (2012).
42. Kirchhausen, T., Macia, E. & Pelish, H. E. Use of dynasore, the small molecule inhibitor of dynamin, in the regulation of endocytosis. *Methods Enzymol.* **438**, 77–93 (2008).
43. Preta, G., Cronin, J. G. & Sheldon, I. M. Dynasore—Not just a dynamin inhibitor. *Cell. Commun. Signal.* **13**, 24 (2015).
44. Nichols, B. Caveosomes and endocytosis of lipid rafts. *J. Cell. Sci.* **116**, 4707–4714 (2003).
45. Takei, K., Yoshida, Y. & Yamada, H. Regulatory mechanisms of dynamin-dependent endocytosis. *J. Biochem.* **137**, 243–247 (2005).
46. Kay, R. R. Macropinocytosis biology and mechanisms. *Cells Dev.* **168**, 203713 (2021).
47. Ivanov, A. I. Pharmacological inhibition of endocytic pathways: is it specific enough to be useful? In *Exocytosis and Endocytosis* (ed Ivanov, A. I.) 15–33 (Humana, 2008).
48. Comisso, C. et al. Macropinocytosis of protein is an amino acid supply route in ras-transformed cells. *Nature* **497**, 633–637 (2013).
49. Albrecht, L. V. et al. GSK3 inhibits macropinocytosis and lysosomal activity through the wnt destruction complex machinery. *Cell. Rep.* **32**, 107973 (2020).
50. Steffan, J. J., Snider, J. L., Skalli, O., Welbourne, T. & Cardelli, J. A. Na<sup>+</sup>/H<sup>+</sup> exchangers and RhoA regulate acidic extracellular pH-induced lysosome trafficking in prostate cancer cells. *Traffic* **10**, 737–753 (2009).
51. Blees, A. et al. Structure of the human MHC-I peptide-loading complex. *Nature* **551**, 525–528 (2017).
52. Shi, G. P. et al. Role for cathepsin F in invariant chain processing and major histocompatibility complex class II peptide loading by macrophages. *J. Exp. Med.* **191**, 1177–1186 (2000).
53. Bryant, P. W., Lennon-Duménil, A. M., Fiebiger, E., Lagaudrière-Gesbert, C. & Ploegh, H. L. Proteolysis and antigen presentation by MHC class II molecules. *Adv. Immunol.* **80**, 71–114 (2002).
54. Somoza, J. R., Palmer, J. T. & Ho, J. D. The crystal structure of human cathepsin F and its implications for the development of novel immunomodulators. *J. Mol. Biol.* **322**, 559–568 (2002).
55. Gorza, L. & Vitadello, M. Grp94 (HSP90B1). In *Encyclopedia of Signaling Molecules* (ed Choi, S.) 2276–2287 (Springer, 2018).
56. Labrador-Garrido, A. et al. Chaperome screening leads to identification of Grp94/Gp96 and FKBP4/52 as modulators of the  $\alpha$ -nuclein-elicited immune response. *Faseb J.* **30**, 564–577 (2016).
57. Murshid, A., Gong, J. & Calderwood, S. K. The role of heat shock proteins in antigen cross presentation. *Front. Immunol.* **3**, 63 (2012).

58. Robert, J., Ramanayake, T., Maniero, G. D., Morales, H. & Chida, A. S. Phylogenetic conservation of glycoprotein 96 ability to interact with CD91 and facilitate antigen cross-presentation. *J. Immunol.* **180**, 3176–3182 (2008).
59. Berwin, B., Hart, J. P., Pizzo, S. V. & Nicchitta, C. V. Cutting edge: CD91-independent cross-presentation of GRP94(gp96)-associated peptides. *J. Immunol.* **168**, 4282–4286 (2002).
60. Sánchez-Pulido, L., Martín-Belmonte, F., Valencia, A. & Alonso, M. A. MARVEL: a conserved domain involved in membrane apposition events. *Trends Biochem. Sci.* **27**, 599–601 (2002).
61. Burr, M. L. et al. CMTM6 maintains the expression of PD-L1 and regulates anti-tumour immunity. *Nature* **549**, 101–105 (2017).
62. Miao, B. et al. CMTM6 shapes antitumor T cell response through modulating protein expression of CD58 and PD-L1. *Cancer Cell* **41**, 1817–1828e1819 (2023).
63. Malmström, M., Jentoft, S., Gregers, T. F. & Jakobsen, K. S. Unraveling the evolution of the Atlantic Cod's (*Gadus morhua* L.) alternative immune strategy. *PLoS ONE* **8**, e74004 (2013).
64. Kleijmeer, M. et al. Reorganization of multivesicular bodies regulates MHC class II antigen presentation by dendritic cells. *J. Cell. Biol.* **155**, 53–63 (2001).
65. van Niel, G. et al. Dendritic cells regulate exposure of MHC class II at their plasma membrane by Oligoubiquitination. *Immunity* **25**, 885–894 (2006).
66. ten Broeke, T., Wubbolts, R. & Stoorvogel, W. MHC class II antigen presentation by dendritic cells regulated through endosomal sorting. *Cold Spring Harb. Perspect. Biol.* **5**, a016873 (2013).
67. Yadati, T., Houben, T., Bitorina, A. & Shiri-Sverdlov, R. The Ins and outs of cathepsins: physiological function and role in Disease Management. *Cells* **9** (2020).
68. Conus, S. & Simon, H. U. Cathepsins and their involvement in immune responses. *Swiss Med. Wkly.* **140**, w13042 (2010).
69. Blander, J. M. Different routes of MHC-I delivery to phagosomes and their consequences to CD8 T cell immunity. *Semin Immunol.* **66**, 101713 (2023).
70. Guermónprez, P. et al. ER-phagosome fusion defines an MHC class I cross-presentation compartment in dendritic cells. *Nature* **425**, 397–402 (2003).
71. Houde, M. et al. Phagosomes are competent organelles for antigen cross-presentation. *Nature* **425**, 402–406 (2003).
72. Mayor, S., Parton, R. G. & Donaldson, J. G. Clathrin-independent pathways of endocytosis. *Cold Spring Harb. Perspect. Biol.* **6** (2014).
73. Cebrian, I. et al. Sec22b regulates phagosomal maturation and antigen crosspresentation by dendritic cells. *Cell* **147**, 1355–1368 (2011).
74. Ellesat, K. S., Yazdani, M., Holth, T. F. & Hylland, K. Species-dependent sensitivity to contaminants: an approach using primary hepatocyte cultures with three marine fish species. *Mar. Environ. Res.* **72**, 216–224 (2011).
75. Holth, T. F. et al. Environmentally realistic exposure to weathered North Sea oil: sublethal effects in Atlantic Cod (*Gadus morhua*) and turbot (*Scophthalmus maximus*). *J. Toxicol. Environ. Health A* **80**, 895–906 (2017).
76. Elbaz-Alon, Y. et al. PDZD8 interacts with Protrudin and Rab7 at ER-late endosome membrane contact sites associated with mitochondria. *Nat. Commun.* **11**, 3645 (2020).
77. Bulankina, A. V. et al. TIP47 functions in the biogenesis of lipid droplets. *J. Cell. Biol.* **185**, 641–655 (2009).
78. Skjeldal, F. M. et al. The fusion of early endosomes induces molecular-motor-driven tubule formation and fission. *J. Cell. Sci.* **125**, 1910–1919 (2012).
79. Raiborg, C., Wesche, J., Malerød, L. & Stenmark, H. Flat clathrin coats on endosomes mediate degradative protein sorting by scaffolding hrs in dynamic microdomains. *J. Cell. Sci.* **119**, 2414–2424 (2006).
80. Falcón-Pérez, J. M., Nazarian, R., Sabatti, C. & Dell'Angelica, E. C. Distribution and dynamics of Lamp1-containing endocytic organelles in fibroblasts deficient in BLOC-3. *J. Cell. Sci.* **118**, 5243–5255 (2005).
81. Blott, E. J., Bossi, G., Clark, R., Zvelebil, M. & Griffiths, G. M. Fas ligand is targeted to secretory lysosomes via a proline-rich domain in its cytoplasmic tail. *J. Cell. Sci.* **114**, 2405–2416 (2001).
82. Progidia, C., Nielsen, M. S., Koster, G., Buccì, C. & Bakke, O. Dynamics of Rab7b-Dependent transport of sorting receptors. *Traffic* **13**, 1273–1285 (2012).
83. Brudal, E. et al. Establishment of three Francisella infections in zebrafish embryos at different temperatures. *Infect. Immun.* **82**, 2180–2194 (2014).
84. Bolte, S. & Cordelières, F. P. A guided tour into subcellular colocalization analysis in light microscopy. *J. Microsc.* **224**, 213–232 (2006).
85. Grimholt, U. et al. A comprehensive analysis of teleost MHC class I sequences. *BMC Evol. Biol.* **15**, 32 (2015).
86. Camacho, C. et al. BLAST+: architecture and applications. *BMC Bioinform.* **10**, 421 (2009).
87. Kumar, S., Stecher, G. & Tamura, K. MEGA7: Molecular evolutionary genetics analysis version 7.0 for bigger datasets. *Mol. Biol. Evol.* **33**, 1870–1874 (2016).
88. Dobin, A. et al. STAR: ultrafast universal RNA-seq aligner. *Bioinformatics* **29**, 15–21 (2013).
89. Robinson, M. D., McCarthy, D. J. & Smyth, G. K. edgeR: a Bioconductor package for differential expression analysis of digital gene expression data. *Bioinformatics* **26**, 139–140 (2010).
90. Love, M. I., Huber, W. & Anders, S. Moderated estimation of Fold change and dispersion for RNA-seq data with DESeq2. *Genome Biol.* **15**, 550 (2014).
91. Perez-Riverol, Y. et al. The PRIDE database resources in 2022: a hub for mass spectrometry-based proteomics evidences. *Nucleic Acids Res.* **50**, D543–D552 (2022).

## Acknowledgements

We acknowledge the NorMIC Oslo imaging platform (Department of Biosciences, University of Oslo), funded by the Research Council of Norway INFRASTRUKTUR-program (project number: 245928). In particular, we thank Frode M. Skjeldal, and Sathiaruby Sivaganesh for excellent technical assistance. We are grateful to Tor Gjoen and his research group, at the Department of Pharmacy, University of Oslo, for providing protocols for transfecting fish cells, and Hanne C. Winther-Larsen, at the Department of Pharmacy, University of Oslo, for sharing Fnn bacterial strain. We thank Ingviil Jensen (at The Arctic University of Norway) and Øyvind Hansen, at Nofima, for kindly providing the ACL cell line. We are grateful to Finn-Eirik Johansen for helpful discussions on Atlantic cod immunology and for the initial arrangements necessary for working with the ACL cells. We acknowledge the Proteomics Core Facility and Manuel Ramirez Garrastacho (Department of Biosciences, University of Oslo) for assisting in experimental procedures and analysis. This facility is a member of the National Network of Advanced Proteomics Infrastructure (NAPI), which is funded by the Research Council of Norway INFRASTRUKTUR-program (project number: 295910). We also thank the crew of R/V Trygve Braarud. At last, we are thankful for the financial support provided by Statsminister Gunnar Knudsen og hustru Sofie født Cappelens familieleगत, the S.G. Sønneland Foundation and COMPARE (funded by UiO).

### Author contributions

Conceptualization: CP, SAB, MHS, KSJ, SJ, and OB. Investigation: SAB, PK. Validation: SAB, PK. Formal analysis: SAB and MHS. Methodology: SAB, MHS, BT, KH. Resources: CP, BT, KH, OB. Funding acquisition: CP, SAB, KSJ, and SJ. Project administration: CP. Writing—original draft preparation: SAB and CP. Writing—review and editing: MHS, BT, KH, KSJ, SJ, and OB.

### Declarations

#### Competing interests

The authors declare no competing interests.

#### Additional information

**Supplementary Information** The online version contains supplementary material available at <https://doi.org/10.1038/s41598-024-76225-z>.

**Correspondence** and requests for materials should be addressed to C.P.

**Reprints and permissions information** is available at [www.nature.com/reprints](http://www.nature.com/reprints).

**Publisher's note** Springer Nature remains neutral with regard to jurisdictional claims in published maps and institutional affiliations.

**Open Access** This article is licensed under a Creative Commons Attribution-NonCommercial-NoDerivatives 4.0 International License, which permits any non-commercial use, sharing, distribution and reproduction in any medium or format, as long as you give appropriate credit to the original author(s) and the source, provide a link to the Creative Commons licence, and indicate if you modified the licensed material. You do not have permission under this licence to share adapted material derived from this article or parts of it. The images or other third party material in this article are included in the article's Creative Commons licence, unless indicated otherwise in a credit line to the material. If material is not included in the article's Creative Commons licence and your intended use is not permitted by statutory regulation or exceeds the permitted use, you will need to obtain permission directly from the copyright holder. To view a copy of this licence, visit <http://creativecommons.org/licenses/by-nc-nd/4.0/>.

© The Author(s) 2024